Continuous structural phase transition and antiferromagnetic order in ilmenite-type $NiVO_3$

Hajime Yamamoto,[1,*] Osamu Ikeda,[2] Takashi Honda,[3] Kenta Kimura,[4] Takuya Aoyama,[5] Kenya Ohgushi,[5] Akio Suzuki,[2] Kenji Ishii,[6] Daiju Matsumura,[7] Takuya Tsuji,[7] Shintaro Kobayashi,[8] Shogo Kawaguchi,[8] Matteo d'Astuto,[9] and Tadashi Abukawa[10,1]

[1]*Institute of Multidisciplinary Research for Advanced Materials, Tohoku University, 2-1-1 Katahira, Aoba-ku, Sendai, Miyagi 980-8577, Japan*

[2]*Department of Earth Science, Graduate School of Science, Tohoku University, 6-3 Aramaki-Aoba, Aoba-ku, Sendai, Miyagi 980-8578, Japan*

[3]*Institute of Materials Structure Science, High Energy Accelerator Research Organization (KEK), 1-1 Oho, Tsukuba, Ibaraki 305-0801, Japan*

[4]*Department of Materials Science, Graduate School of Engineering, Osaka Metropolitan University, 1-1 Gakuen-cho, Nakaku, Sakai, Osaka 599-8531, Japan*

[5]*Department of Physics, Graduate School of Science, Tohoku University, 6-3 Aramaki-Aoba, Aoba-ku, Sendai, Miyagi 980-8578, Japan*

[6]*Kansai Institute for Photon Science, National Institutes for Quantum Science and Technology (QST), 1-1-1 Kouto, Sayo-cho, Sayo-gun, Hyogo 679-5198, Japan*

[7]*Japan Atomic Energy Agency (JAEA), 1-1-1 Kouto, Sayo-cho, Sayo-gun, Hyogo 679-5198, Japan*

[8]*Japan Synchrotron Radiation Research Institute (JASRI), 1-1-1 Kouto, Sayo-cho, Sayo-gun, Hyogo 679-5198, Japan*

[9]*Université Grenoble-Alpes, CNRS, Grenoble INP, Institut Néel, F-38000 Grenoble, France*

[10]*International Center for Synchrotron Radiation Innovation Smart, Tohoku University, 2-1-1 Katahira, Aoba-ku, Sendai, Miyagi 980-8577, Japan*

(Received 27 March 2024; accepted 30 July 2024; published 3 September 2024)

We investigate the crystal and electronic structures as well as magnetic properties of ilmenite-type $NiVO_3$, which has attracted research interest as an $S = 1$ honeycomb lattice magnet. Ilmenite-type $NiVO_3$ samples were synthesized under high-pressure and high-temperature conditions. Synchrotron x-ray diffraction and Rietveld refinement results demonstrated that $NiVO_3$ underwent a continuous structural phase transition from the triclinic ($P\bar{1}$) phase to the rhombohedral ($R\bar{3}$) phase at 450 K. This transition is concomitant with the decomposition of the V-V dimers formed by the tetravalent V ions. X-ray absorption spectroscopy measurements confirmed that the Ni and V ions were divalent and tetravalent, respectively. Magnetic and specific heat measurements revealed that $NiVO_3$ underwent an antiferromagnetic transition at 140 K, and a zigzag-type magnetic order with magnetic propagation vector $k = (0, 1/2, 0)$ was observed by neutron diffraction measurements.

DOI: 10.1103/PhysRevMaterials.8.094402

I. INTRODUCTION

Ilmenite-type vanadium oxides ($A^{2+}V^{4+}O_3$) form only under high-pressure and high-temperature conditions but can be recovered at ambient pressure and room temperature [1–6]. Some of these compounds undergo a fascinating structural transition induced by the formation of direct bonds between the V ions [1]. The ideal ilmenite-type structure (ABO_3) exhibits a rhombohedral symmetry and consists of alternating layers of edge-sharing AO_6 and BO_6 octahedra, with A-site and B-site cations forming honeycomb lattices. Ilmenite-type vanadium oxides such as $MgVO_3$, $CoVO_3$, and $MnVO_3$ exhibit triclinic distortion resulting from the deformation of honeycomb lattices [1–6], which diminishes one of the three parallel V-V lengths of the V honeycombs, causing V-V dimerization. These compounds undergo a structural transition from the triclinic to the rhombohedral phase at approximately 500 K [1,4,6,7]. V-V dimers are not present in the high-temperature phase. In ilmenite-type $MgVO_3$, the structural transition is accompanied by insulator-to-metal and nonmagnetic-to-paramagnetic transitions, indicating the formation of molecular orbitals between adjacent V ions [1,8].

Ilmenite-type vanadium oxides are also of interest for honeycomb lattice magnets. Owing to V-V dimerization, the vanadium ions become nonmagnetic, and the trigonal symmetry of the crystal structure is broken. These compounds can be regarded as distorted honeycomb lattice magnets when the divalent cations (A^{2+}) are magnetic. Ilmenite-type $CoVO_3$ undergoes an antiferromagnetic transition at 140 K, and the Co^{2+} ion exhibits an $S = 3/2$ state [4]. The Co^{2+} spins are arranged in a zigzag-type order, originating from geometrical frustration or interlayer interaction [9,10]. The application of high magnetic fields causes a transition from the antiferromagnetic phase to a weak ferromagnetic phase, which

*Contact author: hajime.yamamoto.a2@tohoku.ac.jp

may be accompanied by a change in structural symmetry. In ilmenite-type $MnVO_3$, Mn^{2+} ($S = 5/2$) adopts a Néel-type antiferromagnetic order below 70 K and exhibits a weak ferromagnetic behavior [7]. By replacing the divalent A^{2+} cations, the magnetic properties of ilmenite-type vanadium oxides can be varied.

Ilmenite-type $NiVO_3$ is an $S = 1$ analog of $CoVO_3$ ($S = 3/2$) and $MnVO_3$ ($S = 5/3$). Synthesis of ilmenite-type $NiVO_3$ was first reported in the 1970s [5]. The ilmenite-type phase was synthesized at 6–6.5 GPa and 1673 K. $NiVO_3$ exhibits a triclinic structure [3] similar to other ilmenite-type vanadium oxides. However, the crystal structure has not yet been determined, and it is still unclear whether V-V dimers are present. A previous study reported that $NiVO_3$ exhibited an antiferromagnetic transition at 153 K. Despite the interest in $NiVO_3$ as an $S = 1$ honeycomb lattice magnet, its crystal, electronic, and magnetic structures are still unclear.

Herein, we describe the crystal structure, electronic state, and magnetic structure of ilmenite-type $NiVO_3$. The $NiVO_3$ samples were synthesized under higher-pressure conditions of 8–9 GPa than previously reported, but at the same and high temperature of 1673 K, to improve the sample quality. The crystal structure of $NiVO_3$ was determined using synchrotron x-ray diffraction (SXRD). V-V dimers were arranged in a ladderlike pattern within the V-honeycomb lattice. The dimer length was 2.717(4) Å at 300 K. The V-V dimers disappeared above 450 K, which was accompanied by a continuous structural transition from the triclinic to the rhombohedral phase. Magnetic susceptibility measurements and x-ray absorption spectroscopy (XAS) of the Ni K and V K edges confirmed that the Ni and V ions were in the +2 and +4 valence states, respectively, in $NiVO_3$. Neutron powder diffraction was performed to reveal the magnetic structure, and it was found that the Ni spins adopted a zigzag-type antiferromagnetic order within the honeycomb lattice.

II. EXPERIMENTAL

$NiVO_3$ samples were synthesized at 8–9 GPa and 1673 K using Walker-type and Kawai-type multianvil apparatuses [11]. The obtained samples were ground in an agate mortar. SXRD measurements were conducted at a temperature range of 100–600 K at BL02B2, SPring-8, with a wavelength of $\lambda = 0.500$ Å. Rietveld analysis was performed using the RIETAN-FP program [12]. The crystal structure was drawn using the VESTA-3 program [13]. XAS measurements of the K edges of Ni and V at room temperature were performed using the transmission method at BL14B1, SPring-8. The temperature dependence of the magnetic susceptibility of the $NiVO_3$ sample was measured using superconducting quantum interference device magnetometers (MPMS-XL and MPMS-3, Quantum Design). The heat capacity measurement was performed at 0 T in a temperature range from 2 to 200 K by a relaxation method using a physical property measurement system (Quantum Design). Neutron powder diffraction measurements were conducted at 20, 50, 80, 110, and 200 K using the BL21 NOVA diffractometer at the Japan Photon Accelerator Research Complex (J-PARC). The exposure time was 4 h at each temperature. Magnetic structure refinement was performed using the FullProf program [14].

III. RESULTS AND DISCUSSION

Crystal structure and V-V dimerization. Ilmenite-type $NiVO_3$ was successfully synthesized under high-pressure and high-temperature conditions. SXRD measurements were performed to determine the crystal structures. Figures 1(a) and 1(b) show the patterns and refinement results obtained at 300 and 600 K, respectively. The determined structural and lattice parameters are presented in Tables S1–S6 of the Supplemental Material [15]. The SXRD pattern at 300 K is in agreement with the triclinic structure, which is the same as that of other ilmenite-type vanadium oxides. Its crystal structure is shown in Fig. 1(c). The occupancies of Ni and V ions were fixed to be 1, because the cation antisite disorder was not detected by the Rietveld analysis of the SXRD data at 100 K. Small amounts of impurities, including NiO and VO_2, were also observed. The NiO phase fraction was approximately 8 wt %. The valences of the Ni and V ions were estimated to be 2.024+ and 3.959+, respectively, using the bond valence sum (BVS) method [16], which indicates the valence state of $Ni^{2+}\,V^{4+}\,O_3$. The V-V dimers were arranged in a ladderlike pattern and the dimer length was 2.717(4) Å. This value is shorter than that of $MgVO_3$ (2.779(7) Å [1]), $CoVO_3$ (2.736(11) Å [4]), and $MnVO_3$ (2.8417(11) Å [6]). The reason for this trend can originate from the difference in the ionic radii, with 0.69 Å for Ni^{2+}, 0.72 Å for Mg^{2+}, 0.745 Å for Co^{2+} (high spin), and 0.83 Å for Mn^{2+} (high spin) [17]. A rhombohedral structure is observed at 600 K, as shown in Fig. 1(b). To confirm the structural transition temperature, SXRD measurements were conducted in the temperature range 100–600 K, as shown in Figs. 2(a) and 2(b). Peak splitting derived from the triclinic distortion decreased with increasing temperature, and the rhombohedral phase appeared above 450 K. This transition was reversible and most likely accompanied by an insulator-to-metal transition. A continuous structural change was observed for $NiVO_3$, suggesting a second-order phase transition, whereas discontinuous transitions were reported for $MgVO_3$, $CoVO_3$, and $MnVO_3$. The temperature dependencies of the lattice parameters are shown in Figs. 2(c) and 2(d). The triclinic distortion decreased rapidly above 350 K. The change in the V-V dimer length with temperature as determined by Rietveld refinement is shown in Fig. 2(e), which indicates that the dimer length increased with temperature. The V-V dimer is not present in this high-temperature rhombohedral phase.

Although $NiVO_3$ has the shortest V-V dimer length at 300 K among ilmenite-type vanadium oxides, this compound has the lowest structural transition temperature. The small size of the A-site cation resulted in a small unit cell that reduced the V-V distances. Considering the critical distance of the V-V bond (2.94 Å) [18], the overlap of vanadium 3d orbitals can also be present in the rhombohedral phase, resulting in the stabilization of this phase. Furthermore, the similarity of the ionic radii of Ni^{2+} and V^{4+} (0.58 Å [17]) can reduce the internal stress between the honeycomb lattice layers. These characteristics of the crystal structure of $NiVO_3$ may result in the continuous phase transition and the low transition temperature.

Magnetic properties and electronic structure of $NiVO_3$. Figure 3(a) shows the temperature dependence of the

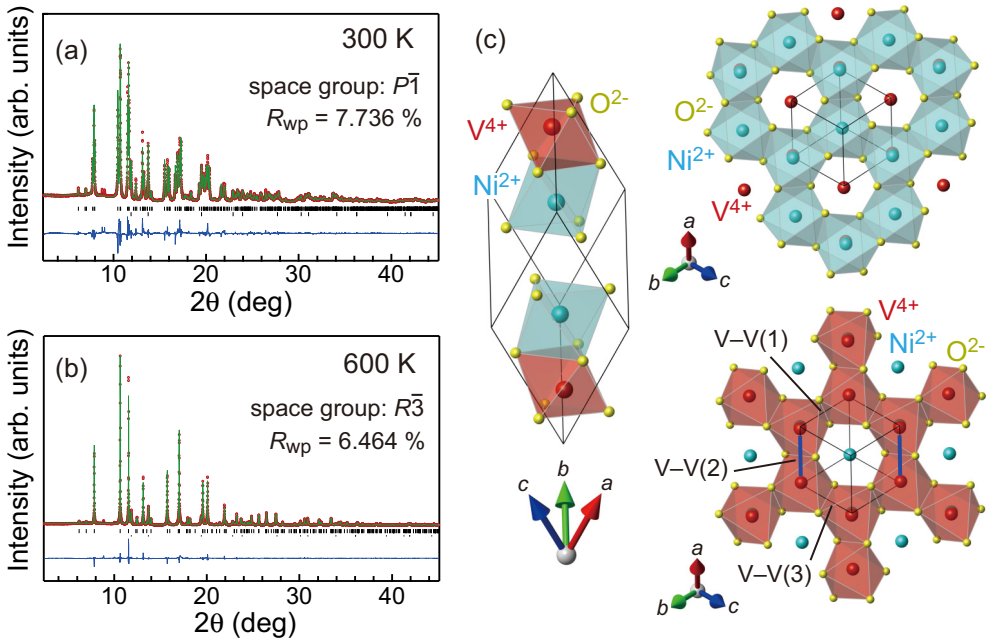

FIG. 1. (a) Rietveld refinement results for the $NiVO_3$ sample at 300 K. The red points and green lines represent the observed and calculated SXRD patterns, respectively, and the blue line denotes their difference. The tick marks indicate the positions of the Bragg reflections of the triclinic $NiVO_3$ (upper) and NiO (lower) phases. (b) Rietveld refinement results for the $NiVO_3$ sample at 600 K. The tick marks indicate the positions of the Bragg reflections of the rhombohedral $NiVO_3$ (upper) and NiO (lower) phases. (c) Crystal structure of $NiVO_3$ at 300 K, showing the NiO_6 (upper) and VO_6 (lower) octahedral layers. The blue lines mark the V-V dimers. Each V-V distance is defined as V-V(1), V-V(2), and V-V(3), respectively.

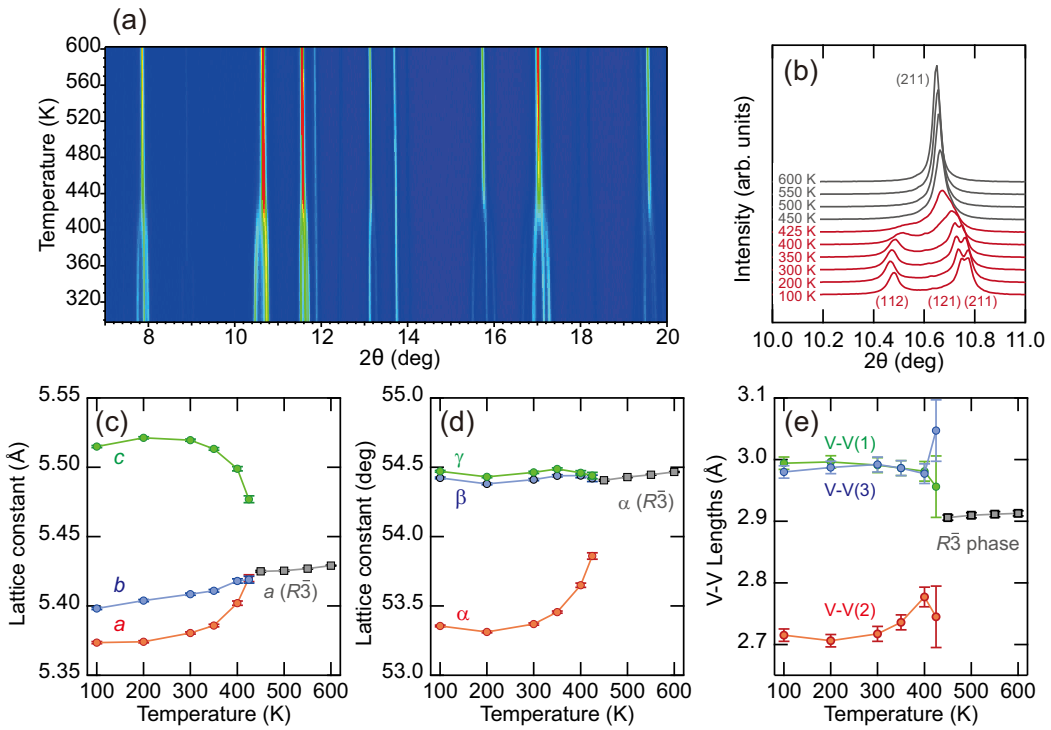

FIG. 2. (a) SXRD patterns of ilmenite-type $NiVO_3$ between 100 and 600 K. (b) SXRD patterns of ilmenite-type $NiVO_3$ at 100, 200, 300, 350, 400, 425, 450, 500, 550, and 600 K. Red and black indicate triclinic and rhombohedral phases, respectively. Reflections from the rhombohedral and triclinic phases were indexed. (c) Temperature dependence of lattice parameters, a, b, and c, obtained from the Rietveld refinement. (d) Temperature dependence of lattice parameters, α, β, and γ, obtained from the Rietveld refinement. (e) Temperature dependence of V-V distances obtained from the refined crystal structure.

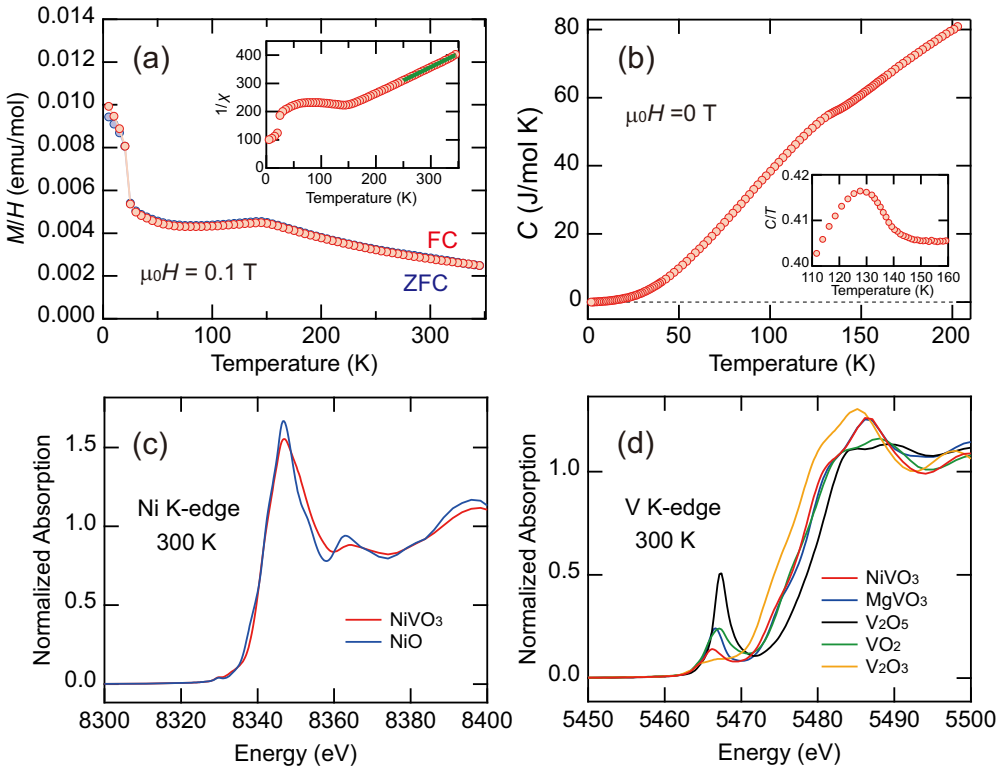

FIG. 3. (a) Temperature dependence of the magnetic susceptibility of ilmenite-type $NiVO_3$ at 0.1 T. Red and blue indicate the field-cooling (FC) and zero-field-cooling (ZFC) processes, respectively. The inset shows the reciprocal plot of the FC process and the result of the Curie-Weiss fitting (green line). (b) Temperature dependence of the specific heat of ilmenite-type $NiVO_3$. The inset shows the data divided by temperature between 110 and 160 K. (c) XAFS spectra of the Ni *K* edges of $NiVO_3$ and NiO at room temperature. (d) XAS spectra of the V *K* edges of $NiVO_3$, $MgVO_3$, V_2O_3, VO_2, and V_2O_5 at room temperature.

magnetic susceptibility and the reciprocal plot of ilmenite-type $NiVO_3$. An antiferromagnetic phase transition was observed at 140 K. A magnetization jump appeared at 25 K. A weak ferromagnetic behavior was observed below the jump temperature, as shown in Fig. S1 [15]. The spontaneous magnetization was approximately $0.001\mu_B$/f.u., which was significantly smaller than the expected value in the case of ferromagnetic or ferrimagnetic orders. To confirm this, the heat capacity was measured, in order to determine whether these behaviors were intrinsic. As shown in the result depicted in Fig. 3(b), a λ-like peak, indicating a second-order phase transition, was observed at approximately 130 K, coincident with the antiferromagnetic transition. No anomalies are observed at 25 K, suggesting that this transition originates from a trace ferromagnetic impurity. The reciprocal magnetic susceptibility appeared almost linear above T_N. The reciprocal plot of magnetic susceptibility from 350 to 250 K was fitted using the Curie-Weiss law, which can be expressed as follows:

$$\frac{1}{\chi} = \frac{T-\theta}{C}, \tag{1}$$

where C is the Curie constant and θ represents the Weiss temperature. The Curie constant is $C = 1.057(6)$ emu/mol, which is identical to the value expected for a system with $S = 1$ ($C = 1.000$ emu/mol in the case of $g = 2$). The Weiss temperature was $\theta = -78(2)$ K, suggesting the presence of antiferromagnetic interaction.

The valence states of the cations in the $NiVO_3$ samples were evaluated using XAS. Figures 3(c) and 3(d) show the XAS spectra of the Ni *K* and V *K* edges at room temperature, respectively, confirming the presence of Ni^{2+} and V^{4+} in $NiVO_3$. From the energy positions of the absorption edges, one can deduce the valence states. Considering that V^{4+} ions become fundamentally nonmagnetic because of the formation of molecular orbitals by analogy with ilmenite-type $MgVO_3$ [1], Ni^{2+} ($3d^8$, $S = 1$) should be responsible for the magnetism in $NiVO_3$. This electronic state coincides with the observed magnetic moment.

Magnetic structure of $NiVO_3$. The neutron powder diffraction patterns and refinement results obtained at 200 and 20 K are shown in Figs. 4(a) and 4(b), respectively. Above the Néel temperature, the nuclear reflections of triclinic ilmenite-type $NiVO_3$ were observed. The crystal structure was identical to that determined from the SXRD data (Table S7 [15]). The impurity phase of NiO and its magnetic reflection ($T_N \sim 425$ K) were also observed. Below the Néel temperature, the additional superlattice reflections, such as (0 1/2 0), (0 1/2 1), (1 1/2 0), ($\bar{1}$ 1/2 0), and (0 1/2 $\bar{1}$), were observed, indicating the presence of commensurate antiferromagnetic order with the propagation vector $k = (0, 1/2, 0)$. The magnetic structure is the same at all temperatures because the magnetic reflection pattern remains unchanged, as shown in Figs. S2–S4 [15]. The intensity of the magnetic reflections increased with decreasing temperature. Considering that $NiVO_3$ crystallizes in $P\bar{1}$ symmetry and that the V ions are nonmagnetic in principle [1],

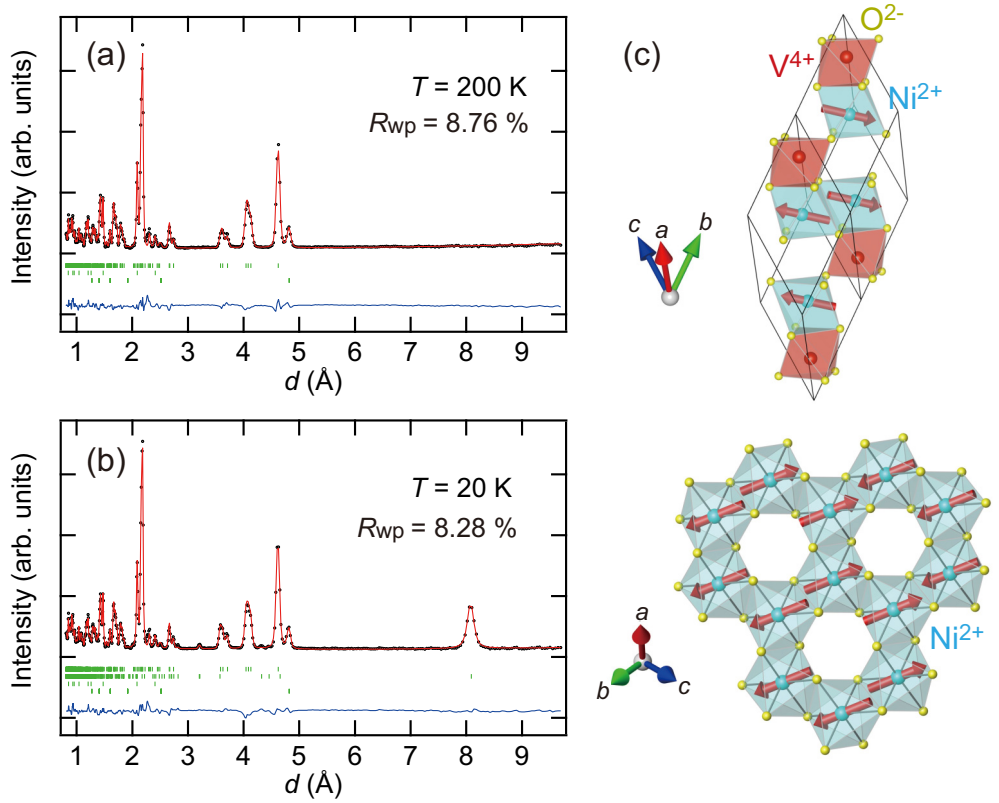

FIG. 4. (a) Neutron powder diffraction patterns and refinement results for ilmenite-type $NiVO_3$ at 200 K. Gray points and red lines denote the observed and calculated patterns, respectively. The difference between these patterns is illustrated by the blue line. Green tick marks indicate the positions of the $NiVO_3$ (top) and the impurity phase of NiO (middle) and its magnetic (bottom) Bragg reflections. (b) Neutron powder diffraction patterns and refinement results for ilmenite-type $NiVO_3$ at 20 K. Green tick marks represent the positions of the $NiVO_3$ nuclear (top), $NiVO_3$ magnetic (second from the top), NiO nuclear (third from the top), and NiO magnetic (bottom) Bragg reflections. (c) Refined magnetic structure of ilmenite-type $NiVO_3$, with the Ni^{2+} spins depicted by red arrows.

the magnetic structure can be expected in that the Ni spins are arranged in a zigzag-type antiferromagnetic order within the honeycomb layer.

The neutron powder diffraction data at 20 K were analyzed assuming the aforementioned structure, as shown in Fig. 4(b). The magnetic space group was defined as $P2s\bar{1}$. The diffraction pattern was well reproduced, and the refined parameters are summarized in Tables S8–S10 [15]. The determined magnetic structure is shown in Fig. 4(c). The Ni spins lie in the xy plane of the NiO_6 octahedron and are oriented in the in-plane direction of the honeycomb. The spins were ferromagnetically ordered in the $[10\bar{1}]$ direction and antiferromagnetically ordered in the perpendicular direction, forming a zigzag-type structure. The obtained magnetic moment of the Ni ion was 1.38 μ_B, which is smaller than the expected value of 2μ_B. The reduction in the ordered magnetic moment may be explained by the presence of spin fluctuations due to geometrical frustration and low dimensionality, which have been observed for various honeycomb lattice antiferromagnets [19–21].

The presence of vanadium ions considerably affects the magnetic properties of $NiVO_3$ despite the formation of nonmagnetic dimers. Ilmenite-type $NiTiO_3$ is an appropriate compound for comparison with $NiVO_3$ owing to the presence of Ti^{4+} ions with a $3d^0$ electronic configuration. The Néel temperature of $NiVO_3$ is significantly higher than that of $NiTiO_3$ ($T_N = 22.5$ K) [22]. Similar trends have been observed for Mn and Co compounds [4,7,23,24], suggesting that the presence of vanadium ions enhanced the interlayer interactions between the Ni honeycomb layers. Indeed, previous studies of other ilmenite-type vanadium oxides, $MnVO_3$ and $CoVO_3$, indicated that the vanadium ions may have a small magnetic moment and they can be magnetically ordered due to the incomplete formation of dimers [7,10]. Below the Néel temperature, $NiTiO_3$ shows A-type antiferromagnetic ordering, in which the Ni spins are ferromagnetically ordered within honeycomb layers and antialigned along the hexagonal c axis [25]. The difference in the magnetic structures of $NiVO_3$ and $NiTiO_3$ implies that the presence of V-V dimers distorts the crystal structure to change the exchange interactions and some of the V moment might affect the magnetic ordering [4,10]. This finding indicates that the V-V dimers not only change the crystal and electronic structure but also have a strong influence on the magnetic properties.

IV. CONCLUSION

In summary, the crystal, electronic, and magnetic structures of ilmenite-type $NiVO_3$ were investigated using synchrotron x-ray and neutron experiments and physical property measurements. V-V dimerization accompanied by a continuous structural transition from the triclinic ($P\bar{1}$) phase to the

rhombohedral ($R\bar{3}$) phase was observed at 450 K. XAS measurements confirmed the presence of Ni^{2+} and V^{4+} ions in this compound. $NiVO_3$ undergoes an antiferromagnetic transition at 140 K, and the Ni^{2+} ions are responsible for the magnetism. Neutron powder diffraction measurements revealed that the Ni spins were arranged in zigzag-type antiferromagnetic ordering within the honeycomb lattice. These findings indicate that V-V dimers have various effects on the crystal structure, electronic states, and magnetic exchange interactions.

ACKNOWLEDGMENTS

This study was supported by Tokuyama Science Foundation, the Grant-in-Aid for Scientific Research (Grants No. JP22H00102, No. JP19H05823, and No. JP19H05822) from the Japan Society for the Promotion of Science (JSPS), the QuantAlps Research Federation, and the GIMRT Program of the Institute for Materials Research, Tohoku University (Proposal No. 202312-CMKOV-0501). Synchrotron x-ray measurements were approved by the Japan Synchrotron Radiation Research Institute (Proposals No. 2023A1728, No. 2023A3657, No. 2023B1635, No. 2023B1583, and No. 2023B3657). Neutron experiments were performed at the Materials and Life Science Experimental Facility of J-PARC under a user program (Proposal No. 2023BF2101). We thank Professor Taku J. Sato, Professor Katsuki Kinjo, Professor Hung-Cheng Wu, and Professor Kazuhiro Nawa for their support with magnetic measurements. We thank Didier Dufeu and Sofien Djellit at the PMag platform of Institut Néel, Grenoble, for their support with magnetic measurements.

[1] H. Yamamoto, S. Kamiyama, I. Yamada, and H. Kimura, J. Am. Chem. Soc. **144**, 1082 (2022).
[2] B. L. Chamberland, P. S. Danielson, and C. W. Moeller, J. Solid State Chem. **26**, 377 (1978).
[3] B. L. Chamberland, J. Solid State Chem. **2**, 521 (1970).
[4] S. Kamiyama, I. Yamada, M. Fukuda, Y. Okazaki, T. Nakamura, T. Nishikubo, M. Azuma, H. Kimura, and H. Yamamoto, Inorg. Chem. **61**, 7841 (2022).
[5] Y. Syono, S. I. Akimoto, and Y. Endoh, J. Phys. Chem. **32**, 243 (1971).
[6] S. Kamiyama, T. Sakakura, H. Kimura, H. Sagayama, S. Kishimoto, I. Yamada, and H. Yamamoto, Cryst. Growth Des. **23**, 2295 (2023).
[7] E. Solana-Madruga, O. Mentré, E. P. Arévalo-López, D. Khalyavin, F. Fauth, A. Missiul, and A. M. Arévalo-López, J. Mater. Chem. C **11**, 9238 (2023).
[8] S. V. Streltsov and D. I. Khomskii, Phys. Usp. **60**, 1121 (2017).
[9] H. Yamamoto, H. C. Wu, A. Miyake, M. Tokunaga, A. Suzuki, T. Honda, and H. Kimura, Appl. Phys. Lett. **123**, 132404 (2023).
[10] E. Solana-Madruga, O. Mentré, A. A. Tsirlin, M. Huvé, D. Khalyavin, C. Ritter, and A. M. Arévalo-López, Adv. Sci. **11**, 2307766 (2024).
[11] D. Walker, M. A. Carpenter, and C. M. Hitch, Am. Mineral. **75**, 1020 (1990).
[12] F. Izumi and K. Momma, Solid State Phenomena **130**, 15 (2007).
[13] K. Momma and F. Izumi, J. Appl. Crystallogr. **44**, 1272 (2011).
[14] J. Rodriguez-Carvajal, Physica B **192**, 55 (1993).
[15] See Supplemental Material at http://link.aps.org/supplemental/10.1103/PhysRevMaterials.8.094402 for refined structural parameters of $NiVO_3$ at 100, 300, and 600 K (SXRD, Tables S1, S3, and S5); lattice parameters and agreement factors of $NiVO_3$ at 100, 300, and 600 K (SXRD, Tables S2, S4, and S6); structural parameters of $NiVO_3$ used for analysis of neutron diffraction data at 200 K (Table S7); lattice parameters and agreement factors of $NiVO_3$ at 200 and 20 K (neutron diffraction, Tables S8 and S9); magnetic field dependence of magnetization of an ilmenite-type $NiVO_3$ sample (Fig. S1); neutron powder diffraction patterns of ilmenite-type $NiVO_3$ at 20, 50, 80, 110, and 200 K (Fig. S2); comparison between the neutron diffraction data of $NiVO_3$ at 25 and 50 K (Fig. S3); and temperature dependence of Ni magnetic moment obtained by magnetic structure refinement (Fig. S4).
[16] I. D. Brown and D. Altermatt, Acta Crystallogr. Sect. B: Struct. Sci **41**, 244 (1985).
[17] R. D. Shannon, Acta Crystallogr. Sect. A **32**, 751 (1976).
[18] J. B. Goodenough, G. Dutta, and A. Manthiram, Phys. Rev. B **43**, 10170 (1991).
[19] J. H. Roudebush, N. H. Andersen, R. Ramlau, V. O. Garlea, R. Toft-Petersen, P. Norby, R. Schneider, J. N. Hay, and R. J. Cava, Inorg. Chem. **52**, 6083 (2013).
[20] A. Yogi, A. K. Bera, A. Maurya, R. Kulkarni, S. M. Yusuf, A. Hoser, A. A. Tsirlin, and A. Thamizhavel, Phys. Rev. B **95**, 024401 (2017).
[21] A. M. Samarakoon, Q. Chen, H. Zhou, and V. O. Garlea, Phys. Rev. B **104**, 184415 (2021).
[22] K. Dey, S. Sauerland, J. Werner, Y. Skourski, M. Abdel-Hafiez, R. Bag, S. Singh, and R. Klingeler, Phys. Rev. B **101**, 195122 (2020).
[23] J. Akimitsu, Y. Ishikawa, and Y. Endoh, Solid State Commun. **8**, 87 (1970).
[24] M. Hoffmann, Phys. Rev. B **104**, 014429 (2021).
[25] G. Shirane, S. J. Pickart, and Y. Ishikawa, J. Phys. Soc. Jpn. **14**, 1352 (1959).